

THREE-SCALAR IMAGING IN TURBULENT NON-PREMIXED FLAMES OF METHANE

JOSEPH FIELDING, ANDREW M. SCHAFFER AND MARSHALL B. LONG

*Department of Mechanical Engineering and Center for Laser Diagnostics
Yale University
New Haven, CT 06520-8284, USA*

Raman scattering from nitrogen in laminar ($Re = 1600$) and turbulent ($Re = 15,000$) non-premixed flames of diluted methane has been investigated as a means of complementing the two-scalar mixture-fraction computation based on measurements of fuel mass fraction and temperature (ξ^{FT}). Using a diluent consisting of argon and oxygen with an overall volumetric dilution ratio of 3/1 (diluent/fuel) allows sufficient variation in the measured nitrogen concentration for its use as a passive scalar. The present experimental setup requires only a single laser (532 nm) in a high-power intracavity configuration. Mixture-fraction profiles calculated using independent fuel-temperature and nitrogen-temperature two-scalar approaches show excellent agreement in the laminar flame. For the turbulent flame, a 100 single-shot average of mixture fraction shows reasonable agreement between the two approaches. Discrepancies are most evident in single-shot images in regions of large mixture fraction ($\xi > \xi_s$) where the nitrogen Raman signal is noise dominated. The location of the stoichiometric contour is consistently determined by both two-scalar approaches. A simple modification of the functional dependence for parameters appearing in the fuel-temperature mixture-fraction formulation is shown to correct deficiencies in the approach predicted by laminar flame calculations, most notably for values of ξ^{FT} around stoichiometric and into lean regimes.

Introduction

Planar imaging of turbulent flames using laser diagnostic techniques such as Lorenz–Mie [1], Rayleigh [2], laser-induced fluorescence [3], and Raman scattering [4] have long been directed toward improved characterization of the flow structures and flame front location. One major goal in studying turbulent flames is to provide quantitative images of mixture fraction ξ , defined as the mass fraction of all atoms originating from the fuel stream. This allows calculation of axial and radial gradient information, and in particular the scalar dissipation χ , which controls the rate of molecular mixing. Experimental data are essential for modelers to construct joint probability density functions conditional on these parameters. Extensive single-point measurements have been made [5]; however, scalar dissipation cannot be extracted because of the lack of spatial gradient data. Line-Raman measurements [6,7] are less restrictive, allowing the computation of one-dimensional scalar dissipation.

One method for constructing a conserved scalar suitable for reacting flows has been through the simultaneous measurement of temperature (T) and fuel concentration [8]. The conserved scalar β is defined based on fuel mass fraction (Y_F) and enthalpy and takes the form

$$\beta = Y_F + c_p T/Q$$

where Q is the lower heat of combustion and c_p is the specific heat at constant pressure. This can be cast into an expression for mixture fraction:

$$\xi^{FT} \equiv \frac{\beta - \beta_{\text{air}}}{\beta_{\text{fuel}} - \beta_{\text{air}}} = \frac{Y_F + c_p(T - T_{\text{air}})/Q}{Y_{F,\text{fuel}} + c_p(T_{\text{fuel}} - T_{\text{air}})/Q}$$

This two-scalar approach, which assumes unity Lewis number and idealized one-step reaction between fuel and oxidizer, relates to the measured signals through

$$\xi^{FT} = \frac{C_1 \sigma}{W \text{Ra}} \text{Rm} + C_2 \frac{c_p}{Q} \left(\frac{\sigma}{\text{Ra}} - T_{\text{air}} \right)$$

where Rm is the measured fuel Raman scattering and Ra is the Rayleigh scattering. The parameter σ , which is proportional to the Rayleigh cross section, the mixture molecular weight W , and the specific heat c_p , are dependent on the mixture fraction. Strained counterflow flame calculations provide appropriate functional forms for these parameters that are incorporated into an iterative scheme for determining ξ . The remaining constants C_1 and C_2 must be determined from calibration experiments.

This approach has been applied successfully [3,9–14]; however, there is a need to improve the certainty in the mixture fraction calculation around the stoichiometric contour. At this location, the fuel concentration approaches zero and the Rayleigh signal

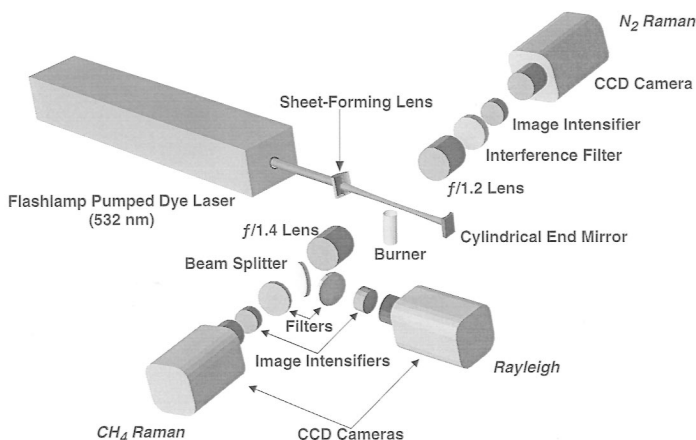


FIG. 1. Schematic of the three-scalar turbulent flame imaging experiment.

remains nearly constant. The acquisition of an appropriate third scalar with continuously varying signal could improve confidence in the two-scalar mixture-fraction calculation in this regime by providing independent quantitative confirmation of the measurements. The present work examines Raman scattering from nitrogen as a third scalar measurement in turbulent non-premixed flames.

In this paper, simultaneous planar Rayleigh, fuel Raman, and nitrogen Raman images have been collected in experiments using three cameras and a single laser. Current detector technology combined with high-energy (~ 5 J/pulse) laser configurations makes Ramanography feasible for molecules such as nitrogen, despite its small scattering cross section [15]. In order for the N_2 Raman channel to provide an independent passive conserved scalar with sufficient signal variation between regions of pure air and pure fuel, experiments were performed in which the fuel stream contained no nitrogen. Assuming no significant nitrogen consumption occurs during reaction, we can write the conserved scalar in terms of nitrogen mass fraction:

$$\beta^{N_2} \equiv Y_{N_2}$$

with the mixture fraction

$$\xi^{N_2} = 1 - \frac{Y_{N_2}}{Y_{N_2,air}} = 1 - \frac{C_3 \sigma}{W Ra} Rm_{N_2}$$

where Rm_{N_2} is the nitrogen Raman signal and C_3 is an additional calibration constant. This formulation requires measurement of the temperature and nitrogen concentration and, thus, represents an additional two-scalar approach.

Experiment

The experimental facility used in the present work to measure Rayleigh, fuel Raman, and nitrogen Raman scattering is shown schematically in Fig. 1. A

single flashlamp-pumped dye laser (Candela LFDL-20; Pyrromethene 546 dye, 2.0×10^{-5} M in methanol) is employed in an intracavity configuration to generate single-shot energies up to 4.7 J at 532 nm. The beam is focused into a sheet by a 30-cm focal-length cylindrical lens, and an 8-mm-wide slit inserted into the cavity provides a beam waist of $500 \mu\text{m}$. Beam waist measurements are performed by imaging the laser sheet from above using Lorenz-Mie scattering from NaCl particles seeded into air with a nebulizer (TSI Model 9306).

Scattered light is collected on both sides of the flame by low $f\#$ camera lenses oriented perpendicular to the laser sheet. The Rayleigh scattering and fuel Raman scattering are collected along the same optical path and divided with a 50/50 pellicle beam splitter, while the weaker nitrogen Raman scattering is collected along the opposite optical path. Image intensifiers are lens coupled to liquid-cooled CCD cameras and isolated with appropriate 10-nm-bandwidth interference filters. The filters and cameras used are 532 nm (center wavelength) for the Rayleigh scattering (Photometrics Star1 CCD), 630 nm for the Stokes-shifted Raman scattering from methane (Photometrics CH250), and 610 nm for nitrogen Raman scattering (Princeton Instruments TE/CCD-512). The image intensifiers are gated for the same 2- μs period to bracket the laser pulse and minimize background interferences from flame luminosity. The experiment is controlled from a single computer that handles the subsequent image transfer and storage. Raw images are corrected for background and throughput as described in Ref. [16].

In the past, the imaging resolution of the optical setup has been characterized in terms of the volume associated with each pixel. For the present work, the pixel volume is $49 \times 49 \times 500 \mu\text{m}^3$, where the largest value corresponds to the laser sheet thickness, and the remaining dimensions describe the area imaged onto a single pixel. The actual spatial

resolution is a more complex function of the optical layout, including alignment, lenses, filters, image intensifiers, and camera pixel size. In order to better quantify the spatial resolution for this configuration, simultaneous images have been taken of a uniformly illuminated 25- μm wire located at the focal plane. Individual camera resolutions are based upon the resulting full-width half-maximum (FWHM) intensity of the wire image from each camera following scaling, translation, rotation, and cropping. The spatial resolution is 170 μm on the Rayleigh camera, 140 μm on the nitrogen Raman camera, and 275 μm on the fuel Raman camera. Translating the wire normal to the plane of the laser sheet within the beam thickness ($\pm 250 \mu\text{m}$ from the focal plane) has minimal effect ($<10\%$) on the individual camera resolutions.

Because this is a multicamera experiment and the cameras are located along different optical trains, there remains the issue of how well the images correlate on a pixel-by-pixel basis. Cross-camera spatial resolutions here are defined based upon adding combinations of matched images from each camera and measuring the resultant FWHM of the wire. With optimal matching, the on-axis spatial resolution is 280 μm , about equal to the largest single-camera resolution. Factors such as distortion may cause degradation away from the optical axis to a maximum measured 400 μm . Using the $1/e^2$ intensity point rather than the FWHM for determining spatial resolution increases the reported values by $\sim 75\%$.

Estimates of the Kolmogorov scale (κ) on the centerline for a diluted methane flame (3/1 air/methane by volume) give a value of $\kappa = 95 \mu\text{m}$ at $Re = 20,600$ [9]. Using this as an approximate value for the turbulent flame in this work, the resolutions reported here are in the range 2–4 κ . A study of an isothermal jet performed by Namazian et al. [17] reports that a spatial resolution of 5 κ should be sufficient for capturing 60% of the scalar dissipation spectrum. In flames, where heat release is expected to increase length scales, a resolution of 5 κ should be sufficient to record most of the scalar dissipation [9].

The burner consists of a 6.1-mm-diameter nozzle surrounded by a 14-mm pilot flame region, which prevents blowoff of the turbulent flames and allows examination of a large range of Reynolds numbers. The premixed pilot flame is fueled by stoichiometric acetylene-hydrogen-air in proportions such that the mixture carbon-hydrogen ratio matches that of the main jet, which allows the flame to be modeled as a two-stream mixing problem [18]. A filtered ambient air coflow ($\sim 7 \text{ m/s}$) prevents entrainment of dust into the flame that would interfere with the Rayleigh measurement. The fuel used in this work is methane mixed with argon and oxygen to provide a 3/1 dilution ratio by volume and a diluent oxygen content to

match that of air. For this fuel composition, the stoichiometric mixture fraction is $\xi_s = 0.41$, which puts the reaction zone well inside the shear layer.

Dilution suppresses much of the soot and formation of soot precursors that can affect the nitrogen Raman signal [19]. In the laminar flame, C_2 fluorescence contributes about 15% to the N_2 Raman signal on the rich side of the flame front when isolated with the 10-nm bandwidth interference filter. Using a narrower 3-nm bandwidth filter centered at a wavelength of 607.3 nm virtually eliminates this interference at a loss of half of the Raman signal. The 3-nm filter is used for the laminar flame results presented in the next section. The broader 10-nm bandwidth filter is used for the turbulent flame imaging to provide maximum SNR, as the interference is expected to be less significant than under laminar flame conditions.

The N_2 Raman images are corrected for temperature dependence of the scattering cross section and the overlap of the Raman spectral profile with the bandpass of the interference filter. Simple convolution of the temperature-dependent Raman spectrum (computed using the Raman code developed by Hassel [20]) with the zero-degree-incidence filter profile gives a correction factor that does not adequately predict the signal variation with temperature. This effect is a consequence of the placement of the interference filter relative to the collection lens. A geometric analysis reveals that off-axis rays entering the filter create a significant shift in the effective spectral profile toward shorter wavelengths. A series of calibration experiments, in conjunction with the geometric analysis, is used to provide the temperature correction. The magnitude of the N_2 Raman correction is as high as 50% at the peak flame temperatures ($T_{\text{ad}} \approx 2200 \text{ K}$) for the 10-nm bandwidth interference filter. This temperature dependence is partly beneficial in that ample N_2 Raman signal is available even at higher temperatures. A similar analysis applied to the methane Raman signal indicates no off-axis ray correction is necessary.

Calibration images are taken before and after each experimental sequence in flows of known uniform concentration (helium, methane, and air). Additionally, a series of measurements performed in a non-reacting jet of fuel issuing into ambient air ($T_1 = T_2 = 298 \text{ K}$) confirms the precision of the temperature images, with maximum fluctuations about the mean of $\pm 10 \text{ K}$ and a signal-noise ratio (SNR) of 70.

Results and Discussion

Images have been obtained from a laminar flame ($Re = 1600$) taken 15 nozzle diameters (D) downstream of the jet exit, and from a turbulent flame ($Re = 15,000$) at a distance 25 D downstream. Data from the laminar flame represent a 50-shot average, which

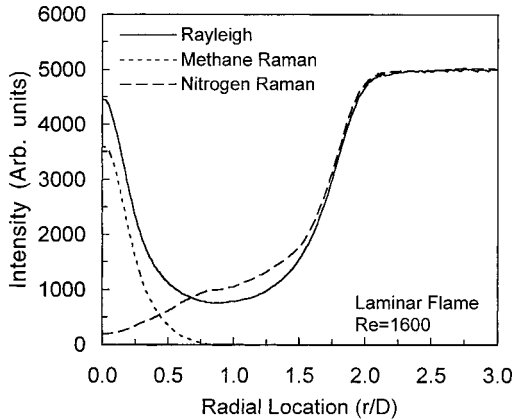


FIG. 2. Line plot (one pixel height) showing radial variation of Rayleigh, fuel Raman, and nitrogen Raman signals in the laminar flame ($Re = 1600$) 15 jet diameters ($D = 6.1$ mm) downstream of the jet exit. The data represent a 50-shot average.

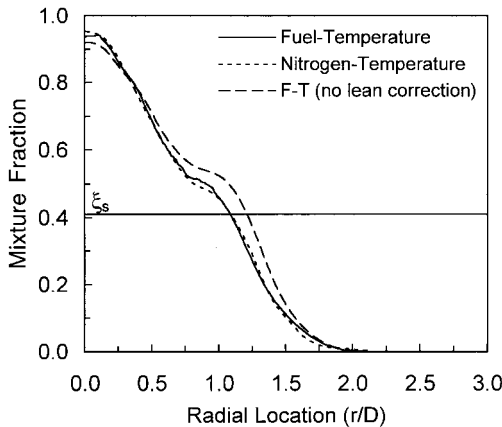


FIG. 3. Radial variation of mixture fraction calculated from fuel-temperature (*solid line*) and nitrogen-temperature (*short dashes*) two-scalar approaches 15 D downstream in the laminar flame. Previous functional dependences of parameters in ξ^{FT} overpredict the fuel-temperature mixture fraction in regions around and lean of stoichiometric (*long dashes*).

gives a Rayleigh SNR of 250 in the ambient air region. Fuel Raman SNR is 30 in the fuel core, and the nitrogen Raman has SNR values of 20 in the ambient air. A contour smoothing technique [21] has been applied to both Raman channels, which improves the fuel Raman SNR by a factor of 2 and the nitrogen Raman by more than a factor of 10.

Figure 2 shows the scattered signals along a line (one pixel height) as a function of the normalized radius. The flattening of the N_2 Raman profile

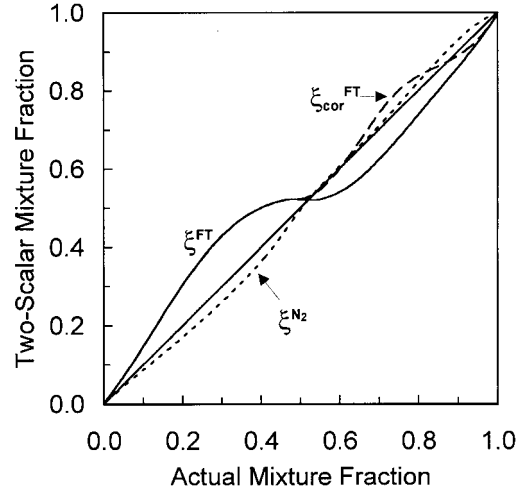


FIG. 4. Mixture fraction calculated from strained laminar flame calculations (100 s^{-1}) using the fuel-temperature (*solid line*) and nitrogen-temperature (*short dashes*) two-scalar approaches plotted against mixture fraction calculated using the formula proposed by Bilger [22]. The effect of fuel correction on ξ^{FT} is also shown (*long dashes*).

around $r/D = 0.75$ is attributable to the temperature sensitivity of the signal; increased spectral overlap with the interference filter occurs at higher temperatures for this experimental setup. Figure 3 shows mixture fraction as a function of radius in the laminar flame computed using fuel-temperature (ξ^{FT}) and nitrogen-temperature (ξ^{N_2}) two-scalar approaches. There is good agreement between the two profiles, and both predict a centerline mixture fraction just over $\xi \approx 0.9$, and the radial location of the stoichiometric contour coincides.

Counterflow flame calculations (strain rate = 100 s^{-1}) of this system demonstrate the departure of the two-scalar formulation from the “actual” mixture fraction (Fig. 4) calculated using the Bilger formula [22]:

$$\xi \equiv$$

$$\frac{2Z_C/W_C + \frac{1}{2}Z_H/W_H + (Z_{O,\text{air}} - Z_O)/W_O}{2Z_{C,\text{fuel}}/W_C + \frac{1}{2}Z_{H,\text{fuel}}/W_H + (Z_{O,\text{air}} - Z_{O,\text{fuel}})/W_O}$$

where Z_i and W_i are the atomic mass fractions and weights, respectively, for carbon (C), hydrogen (H), and oxygen (O). Deviation from one-step chemistry (i.e., loss of parent fuel to intermediate species) is compensated in calculating fuel concentration by the expression $Rm_F = Rm_{F,0}(1 + C_F\Phi^2)$, where $Rm_{F,0}$ is the uncompensated value, and the reactivity is defined as $\Phi = (T - T_{\text{ambient}})/(T_{\text{ad}} - T_{\text{ambient}})$ [12].

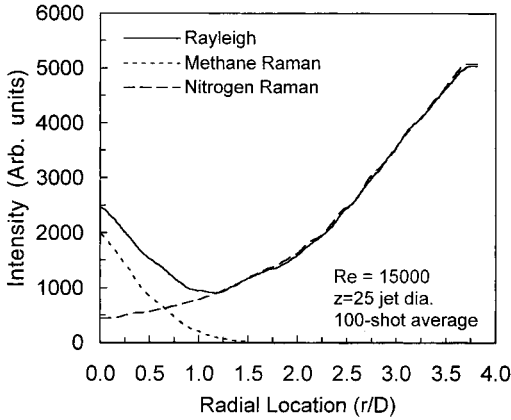


FIG. 5. Measured radial Raman and Rayleigh intensities for a 100-shot average of the turbulent flame ($Re = 15,000$) along a line $25D$ downstream.

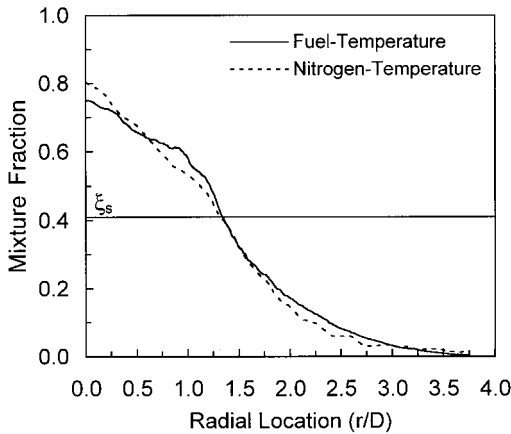


FIG. 6. Radial variation of mixture fraction calculated from fuel-temperature (*solid line*) and nitrogen-temperature (*short dashes*) two-scalar approaches $25D$ downstream in the turbulent flame (100-shot average).

C_F is a weighting coefficient ($C_F = 0.8$) and, as illustrated in the figure by the curve marked ξ_{cor}^{FT} , corrects on the rich side of stoichiometric. The slight plateau in mixture fraction shown in Fig. 3 coincides with the deviation occurring near $\xi^{FT} = 0.5$ in Fig. 4 and spatially coincides with the peak temperature. It is also predicted from the flame calculations that the mixture fraction based upon nitrogen mass fraction should exhibit little deviation from ξ . To correct ξ^{FT} on the lean side, $c_p(\xi)$, $\sigma(\xi)$, and $W(\xi)$ are described as functions of the predicted two-scalar mixture fraction ξ^{FT} , rather than the actual mixture fraction from the flame calculations. The latter approach gives the third curve in Fig. 3 (denoted F-T no lean

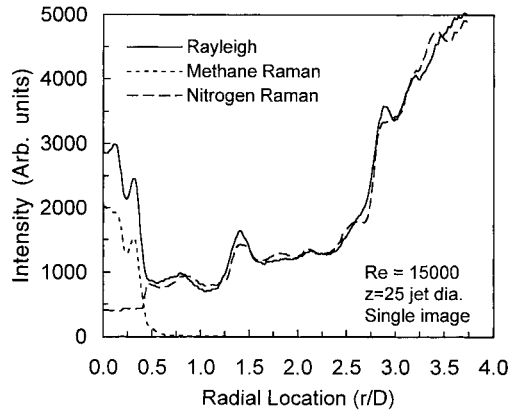


FIG. 7. Measured radial Raman and Rayleigh intensities for a single shot of the turbulent flame along a line $25D$ downstream.

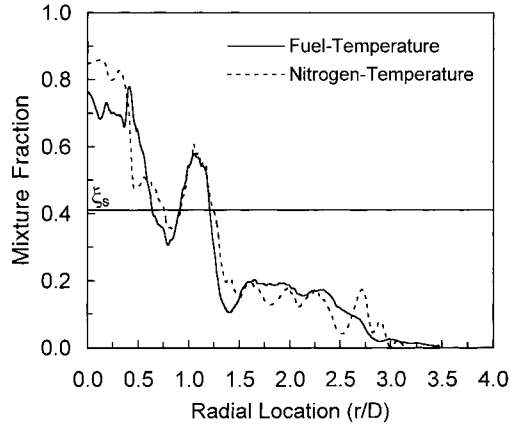


FIG. 8. Radial variation of mixture fraction calculated from fuel-temperature (*solid line*) and nitrogen-temperature (*short dashes*) two-scalar approaches $25D$ downstream in the turbulent flame (single shot).

correction), which overpredicts the mixture fraction—in agreement with the trends indicated in Fig. 4. Without this simple modification, the location of the stoichiometric contour is in error by $0.1D$ toward the lean side. The temperature correction of the N_2 Raman signal causes a minor dependence of ξ_{cor}^{FT} on the value of ξ^{FT} because the latter is used to adjust the Rayleigh cross-section parameter, $\sigma(\xi)$. This effect is small, however, and the magnitude of the temperature correction is reduced by 20% in the turbulent flame measurement because of the larger bandwidth interference filter. The flame computations are insensitive to variations in the strain rate over the range $10\text{--}200\text{ s}^{-1}$, which is expected to be

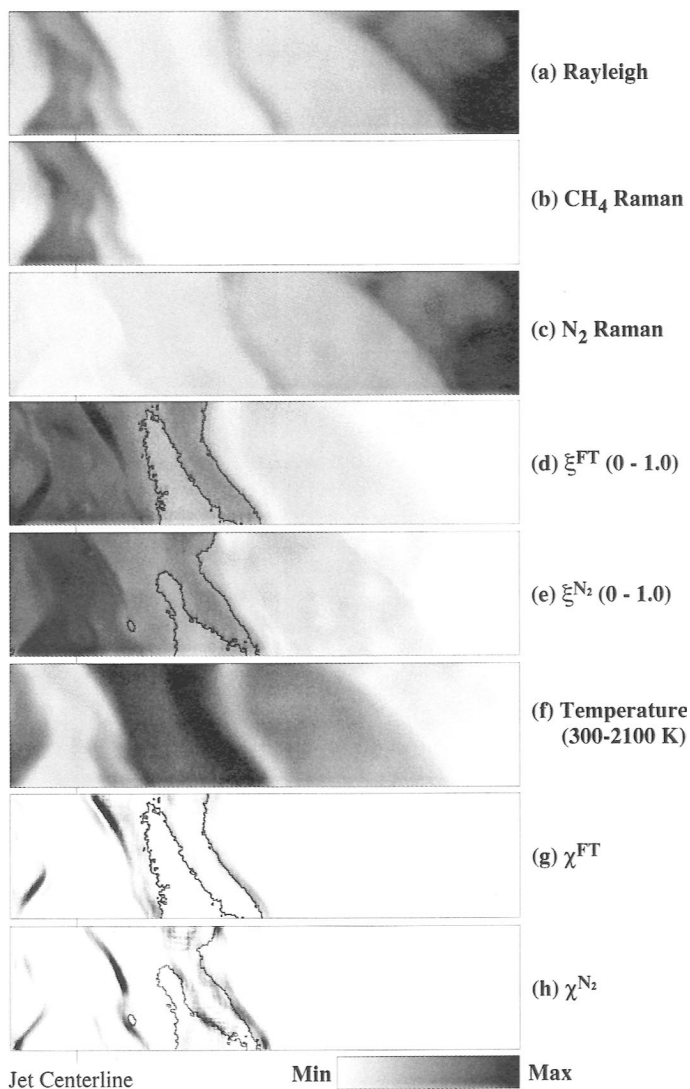


FIG. 9. Instantaneous (a) Rayleigh, (b) CH₄ Raman, and (c) N₂ Raman images of the turbulent flame. Also shown are the computed mixture-fraction images (d) ξ^{FT} , (e) ξ^{N_2} , (f) temperature, and scalar dissipation images (g) χ^{FT} and (h) χ^{N_2} . Image size is $4.3D \times 1D$; data for line plots of Figs. 7 and 8 are taken along the center of each image.

representative of the scalar dissipation values measured in the turbulent flame, based on existing data in similar flames [12,14,21].

For the turbulent flame, 100 instantaneous images were processed and then averaged. Figure 5 shows the Rayleigh and Raman profiles. Comparison of the computed mixture fractions in Fig. 6 shows good agreement between the two approaches, and the location of the stoichiometric contour again coincides. For values $\xi > \xi_s$, there is some discrepancy between the profiles of ξ^{FT} and ξ^{N_2} , and peak centerline mixture fractions are $\xi_{r=0}^{FT} = 0.75$ versus $\xi_{r=0}^{N_2} = 0.80$. These discrepancies may reflect the limitations in ξ^{FT} caused by the deviation from the actual mixture fraction indicated in Fig. 4; however, the

maximum discrepancy between the two profiles has a width of only $0.2D$. Again, failure to parameterize the variables in the two-scalar mixture fraction with respect to predicted ξ^{FT} would have caused a larger discrepancy in the mixture fraction obtained with the different two-scalar techniques.

In order to examine the performance of the different mixture-fraction formulations on a single-shot basis in the turbulent flame, one set of collected signals is shown in Fig. 7, and the derived mixture fractions are shown in Fig. 8. Line plots of mixture fraction reveal that ξ^{N_2} and ξ^{FT} profiles generally agree around stoichiometric, although noise limitations are evident in the nitrogen Raman signal. In the turbulent flame, the N₂ Raman signal has an SNR of 6

before smoothing; this increases to 30 after contour smoothing. Instantaneous images of the turbulent flame are shown in Fig. 9, with an image size of $4.3D \times 1D$. Radial data for Figs. 7 and 8 are taken along the center of each image. Additionally, scalar dissipation (two dimensions) is computed based upon each mixture-fraction formulation, where the scalar dissipation χ is defined as $\chi \equiv 2D\nabla\xi \cdot \nabla\xi$. Temperature variations are accounted for in the diffusivity \mathcal{D} , by the relationship $\mathcal{D} = \mathcal{D}_0 (T/T_0)^{1.67}$. The χ^{N_2} image should be regarded as semiquantitative due to the modest SNR of the nitrogen Raman signal. Qualitatively, the images appear similar, revealing the same main structural features, with peak scalar dissipation apparent along the edge of the main jet. The position of the stoichiometric mixture-fraction contour is highlighted (black lines) in these images.

Conclusions

Two simultaneous methods of imaging mixture fraction have been investigated using planar Rayleigh, fuel Raman, and nitrogen Raman scattering in non-premixed flames using argon-oxygen diluted methane as a fuel. The different approaches are in good agreement when applied to a laminar flame. Here, the nitrogen-temperature mixture fraction served as a guide for correcting the fuel-temperature mixture fraction for values near and lean of stoichiometric. It has been shown that parameterizing specific heat, molecular weight, and Rayleigh cross section as a function of ξ^{FT} predicted from counterflow flame calculations, rather than the actual mixture fraction, dramatically improves the performance of this two-scalar approach. Under turbulent conditions ($Re = 15,000$), the two approaches reveal differences close to the centerline, most likely a result of noise limitations of the nitrogen Raman signal. One of the shortcomings of the two-scalar approach using fuel concentration and Rayleigh scattering is the lack of a strongly varying scalar quantity around the stoichiometric contour. This work has shown that Stokes-shifted nitrogen Raman scattering is a viable candidate for a third scalar quantity to supplement the usual two-scalar approach based on measurements of fuel mass fraction and temperature. By eliminating nitrogen from the fuel stream diluent, the nitrogen mass fraction provides sufficient variation to serve as a passive scalar.

Although modest SNR of the nitrogen Raman make more detailed quantitative and statistical comparisons premature at this point, the current evidence indicates that this technique merits continued investigation. An added benefit of this experimental setup is that only a single laser is required. The ultimate goal of these efforts is to combine three measurements into a comprehensive mixture-fraction

calculation that offers significant improvement over two-scalar techniques, while maintaining the ability to compute gradient information required to accurately determine scalar dissipation.

Acknowledgments

The authors gratefully acknowledge the support of this research by the Air Force Office of Scientific Research (Grant Number F49620-97-1-0096) and would like to thank Dr. Michael Tanoff for assistance with the counterflow flame calculations and Dr. Robert Barlow for his useful suggestions regarding the experiments.

REFERENCES

1. Long, M. B., Chu, B. T., and Chang, R. K., *Opt. Lett.* 16:958-960 (1983).
2. Escoda, M. C. and Long, M. B., *AIAA J.* 21:81 (1983).
3. Kelman, J. B. and Masri, A. R., *Combust. Sci. Technol.* 122:1-32 (1997).
4. Long, M. B., Fourquette, D. C., Escoda, M. C., and Layne, C. B., *Opt. Lett.* 8:244-246 (1983).
5. Masri, A. R., Dibble, R. W., and Barlow, R. S., *Prog. Energy Combust. Sci.* 22:307-362 (1996).
6. Nandula, S. P., Brown, T. M., Pitz, R. W., and DeBarber, P. A., *Opt. Lett.* 19:414-416 (1994).
7. Chen, Y. C. and Mansour, M. S., in *Twenty-Sixth Symposium (International) on Combustion*, The Combustion Institute, Pittsburgh, 1996, pp. 97-103.
8. Stårner, S. H., Bilger, R. W., Dibble, R. W., and Barlow, R. S., *Combust. Sci. Technol.* 86:223-236 (1992).
9. Stårner, S. H., Bilger, R. W., Lyons, K. M., Frank, J. H., and Long, M. B., *Combust. Flame* 99:347-354 (1994).
10. Frank, J. H., Lyons, K. M., Marran, D. F., Long, M. B., Stårner, S. H., and Bilger, R. W., in *Twenty-Fifth Symposium (International) on Combustion*, The Combustion Institute, Pittsburgh, 1994, pp. 1159-1166.
11. Long, M. B., Frank, J. H., Lyons, K. M., Marran, D. F., and Stårner, S. H., *Ber. Bunsen-Ges. Phys. Chem.* 97:1555-1559 (1993).
12. Stårner, S. H., Bilger, R. W., Long, M. B., Frank, J. H., and Marran, D. F., *Combust. Sci. Technol.* 129:141-163 (1997).
13. Kelman, J. B., Masri, A. R., Stårner, S. H., and Bilger, R. W., in *Twenty-Fifth Symposium (International) on Combustion*, The Combustion Institute, Pittsburgh, 1994, pp. 1141-1147.
14. Kelman, J. B. and Masri, A. R., *Combust. Sci. Technol.* 129:17-55 (1997).
15. Marran, D. F., Frank, J. H., Long, M. B., Stårner, S. H., and Bilger, R. W., *Opt. Lett.* 20:791-793 (1995).
16. Long, M. B., in *Instrumentation for Flows with Combustion* (A. M. K. P. Taylor, ed.), Academic, New York, 1993, p. 467.

17. Namazian, M., Schefer, R. W., and Kelly, J., *Combust. Flame* 74:147–160 (1988).
18. Stårner, S. H. and Bilger, R. W., *Combust. Flame* 61:29–38 (1985).
19. Dibble, R. W., Masri, A. R., and Bilger, R. W., *Combust. Flame* 67:189–206 (1987).
20. Hassel, E. P., *RAMSES Spectral Synthesis Code*, University of Darmstadt, 1996.
21. Stårner, S. H., Bilger, R. W., and Long, M. B., *Combust. Sci. Technol.* 107:195–203 (1995).
22. Bilger, R. W., Stårner, S. H., and Kee, R. J., *Combust. Flame* 80:135–149 (1990).

COMMENTS

A. R. Masri, The University of Sydney, Australia. These measurements are very hard to make, and the authors have pushed this field a step forward. The difficulty I have with mixture fraction measurements from Raman N_2 is that, at low mixture fractions, the error increases because you are now subtracting two large numbers. At what stoichiometric mixture fraction is this approach no longer attractive?

Author's Reply. We agree that the mixture fraction measured from N_2 Raman contains some error due to the weak signal levels. This effect is most severe at higher values of mixture fraction. Our fuel diluent contained no nitrogen, which means decreasing signal and signal-to-noise ratio

(SNR) with increasing mixture fraction. Beyond some value of the mixture fraction, the SNR of the N_2 Raman becomes a liability, but this uncertainty is not significantly amplified by the mathematical expression for ξ^{N_2} . We have confidence in our single-shot turbulent flame measurements up through the stoichiometric value of mixture fraction ($\xi_s = 0.41$); beyond this value, the predicted signal level falls below 10% of its ambient air value and should be treated with caution. We were most concerned with the stoichiometric contour and lower values of mixture fraction in the present work because of the discrepancies between ξ^{FT} and ξ predicted by the counterflow calculations in this regime (Fig. 4).